J. Fluid Mech. (1985), *vol.* 156, *pp.* 401–418
Printed in Great Britain

Mean-flow measurements in a supersonic three-dimensional turbulent boundary layer

By ANTHONY DEMETRIADES AND GLENN McCULLOUGH
Montana State University, Bozeman, Montana 59717

(Received 8 November 1983 and in revised form 17 October 1984)

Measurements are presented of the mean flow in a supersonic turbulent boundary layer subjected to a constant weak transverse pressure gradient. The temperature and longitudinal velocity and the axial shear stress were only slightly affected by the three-dimensionality but a clearly defined crossflow component appeared, in the manner suggested by theory and confirmed in earlier experiments. The flow deflection angle and transverse-velocity component achieved a self-preserving form so long as the transverse-pressure gradient remained constant, and both achieved a maximum at the sublayer edge; the deflection angle seemed to decrease again between the latter and the surface. An empirical relation was found between the pressure-gradient strength and the maximum in the crossflow, and the dependence of the latter on distance from the surface was used to test analytical crossflow predictions. The data are in general agreement with Van Den Berg's law of the wall. The data also support the so-called parabolic law following a relaxation distance, especially if inviscid gradients are accounted for, and if the normal coordinate is contracted by the compressibility transformation.

1. Introduction

Boundary-layer flows over most surfaces of aerodynamic interest are three-dimensional in nature in the sense that, within the layer, the total-velocity vector is deflected transversely by an amount dependent on the distance from the surface. This deflection can cause the surface friction and heat transfer to depart drastically from what would occur for an ordinary two-dimensional boundary layer. Substantial progress in calculating three-dimensional effects at low speeds has been made by numerical methods (e.g. Fanneløp & Krogstad 1975; Rastogi & Rodi 1978), and there is good reason to expect that such methods can predict a number of common flow configurations (e.g. Vermeulen 1971; East 1973). Similar comparisons with high-speed data are scarce, however, mainly because such data have not yet been widely available; in fact the only high-speed three-dimensional boundary-layer data available appear to be limited to those from the early experiments of Hall & Dickens (1968) and the more recent work of Yanta, Ausherman & Hedlund (1982).

The present paper provides data which can be used as a testing ground for numerical solutions of the three-dimensional Navier–Stokes equations, but it was also motivated by the opportunity to examine the extension of some early analytical approximations of three-dimensional boundary-layer behaviour to high speeds. Examples of such analyses are the 'parabolic law' discussed by Mager (1952), Cooke (1958), and Braun (1959), the so-called Johnston (1957) polar relation between the crossflow and the longitudinal velocity component, and Van Den Berg's (1975) more recent 'law of the wall' for three-dimensional flows.

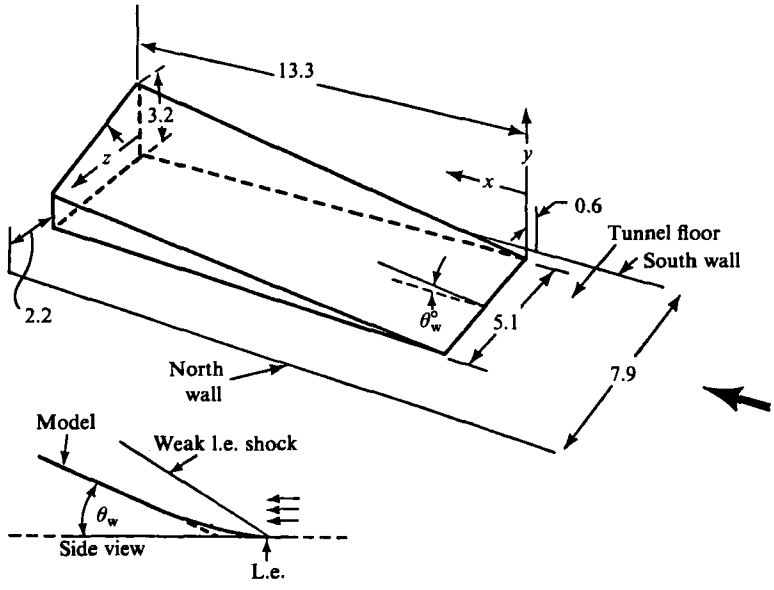

FIGURE 1. Model used for three-dimensional boundary-layer study; dimensions in cm.

To preserve generality, self-preservation of the test flow was sought by imposing a constant transverse-pressure gradient along the streamline on which the measurements were made. Because of the confined space in which the data were collected a novel sensor, based on the Pitot tube principle, was devised. Details of this and the overall experimental arrangement can be found in Demetriades & McCullough (1982), and will be described in the next section.

2. Experimental apparatus

The measurements were carried out in Montana State University's continuous supersonic wind tunnel, which generates a steady, well-calibrated stream of pre-dried air. Flow conditions were fixed at Mach number 3.0, stagnation temperature of 311 K, stagnation pressure of 8×10^4 N/m^2 (600 Torr), and unit Reynolds number of 55000 cm^{-1}. Under these conditions the boundary layer covering the test-section floor was turbulent with a thickness of just under 1 cm. The twisted-wedge model pictured on figure 1 was secured on the floor in such a way that it 'scooped up' this boundary layer. Since the model wedge angle θ_w varied in the lateral (spanwise) direction z, adjacent streamlines arriving at the model leading edge experienced different compression levels as they ascended the wedge. Simple oblique-shock-wave theory was used to prescribe the wedge-angle dependence on z, in such a way that the lateral pressure gradient $\partial p/\partial z$ on the model was constant; at the same time the longitudinal gradient $\partial p/\partial x$ away from the shock wave could theoretically be made nil. Slots cut along the side of the model, pictured on figure 1, served to minimize the interference between the model and the tunnel sidewalls. The model surface pressure produced with this arrangement was found to conform quite closely to that calculated from oblique-shock-wave theory. The values and significance of the pressure gradients generated will be discussed further below.

The measurement of flow direction in the boundary layer was a most critical

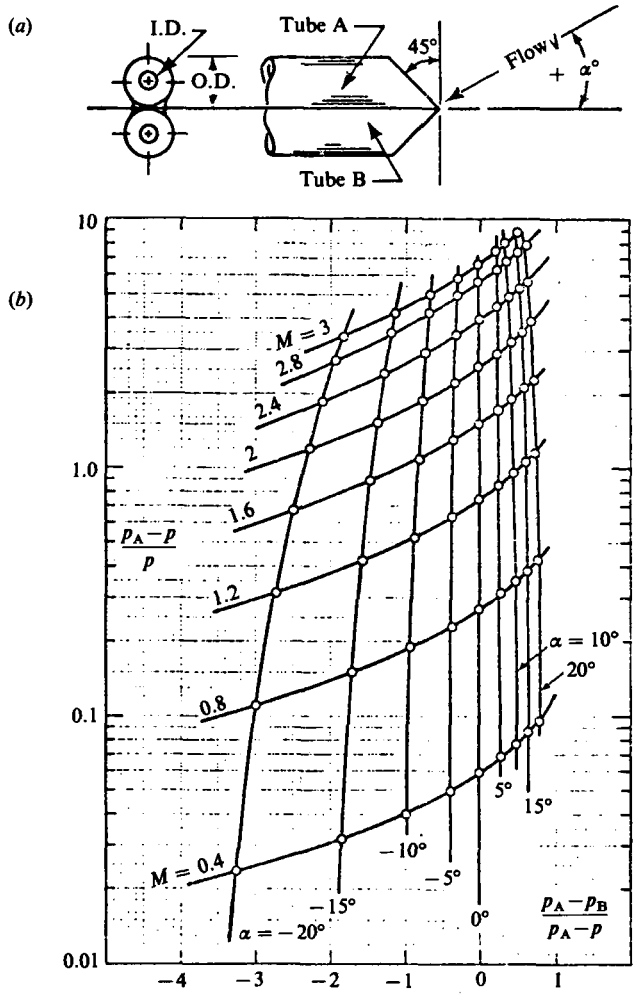

FIGURE 2. (*a*) Yawmeter geometry, with (*b*) calibration algorithm.

problem in this work. Because of the confined working space and small boundary-layer thickness δ (1 cm) one could not introduce rotating probes (Hall & Dickens 1968) or use laterally wide sensors with multiple pitot openings (Spaid, Hurley & Helman 1975). A 'yawmeter' were therefore designed and built, shown in figure 2, which consisted of two 0.015 cm-diameter steel tubes A and B attached side by side, with their openings bevelled in opposite directions at 45°. In principle, Newtonian theory can be used to demonstrate that, if the local static pressure p around the probe tip is known, the pressures p_A and p_B measured with tubes A and B can be used to find the incident Mach number M and the inclination angle between the flow vector and the probe plane of symmetry. Calibrations at $M = 0$ and 3 showed that this approach was valid, provided that a Mach-number-dependent angle $\psi° \simeq 6.9M$ was added to the 45° bevel as a correction. These calibrations were combined to form a computer algorithm, pictured graphically in figure 2, by which the measured p_A, p_B and the static pressure p can be used to find the local Mach number M and incidence angle α at any point in the flow. The measurement error with this technique, which is presented in detail in Demetriades & McCullough (1982), does not exceed $\pm 0.5°$ in α.

In addition to the yawmeter a type K bare-bead thermocouple was used to record the local total temperature. This sensor had a diameter $d = 0.013$ cm and a resolution of 0.25 K, and was calibrated in terms of its Reynolds number based on d to give the actual local total temperature T_{0a} from the measured T_{0m} as follows:

$$\eta \equiv \frac{T_{0m}}{T_{0a}} = \left(1 - \frac{T}{T_{0a}}\right) f(Re_d) + \frac{T}{T_{0a}}, \tag{1}$$

with the recovery factor

$$f(Re_d) = 0.915 + 0.48 \times 10^{-3} (Re_d)^{0.5} - 0.023 \times 10^{-3} Re_d.$$

Finally the surface skin friction was measured with a Preston tube consisting of a 0.1 cm-diameter pitot tube traversed along the surface. Readings from this probe were converted into surface-friction coefficients using the correlation proposed by Bradshaw & Unsworth (1974). It should be noted that this device, as well as the bare-bead thermocouple, had been previously used in the same wind tunnel by Laderman (1980). In the present instance of a smooth, adiabatic wall without streamwise pressure gradient, and with only a weak transverse gradient, the use of the Preston tube is straightforward. The tube was traversed continuously in contact with the model surface following the path of the test streamline, the location of which will be discussed below.

The yawmeter and thermocouple were alternately suspended rigidly above the model and were traversed in a direction vertical to the tunnel floor by an automated electromechanical system integrated into the data-acquisition equipment. The system moves the probe a predetermined distance, pauses to allow equilibration of the sensor reading, and then records digitally the voltage sensed by the probe. The computer programs for data reduction utilized the algorithm shown on figure 2, performed the iterations necessary according to (1) and produced all local flow properties as a function of distance from the model surface.

3. Pressure gradients and the test streamline

One of the design objectives of this experiment was to allow the boundary layer to grow in a region of constant transverse pressure gradient (TPG) without longitudinal (streamwise) variations in pressure or boundary-layer-edge conditions. This required the selection of a 'test' streamline of constant TPG, along which the longitudinal gradients were very small or nil. Transverse-pressure gradients without longitudinal gradients were ensured to a first approximation by the model design, and were checked by static-pressure measurements on the surface. Measurements were then also made with the yawmeter of the flow incidence just outside the boundary layer; a flow direction 'map' was next prepared, and a single boundary-layer-edge streamline was chosen from it, along which detailed data were to be taken.

As expected the flow veered to the left, as seen on figure 3, in response to the overall pressure differences on the model. The test streamline chosen, shown in this figure, is drawn to scale and represents a relatively small turning of the inviscid flow just outside the boundary layer; over a distance of about 8 cm the net streamline deflection (represented by α_e on figure 3) was about 6°. As implied by the figure, data were not taken over the first 4 cm of the model, since a weak shock wave emanating from the model leading edge and its interaction with the layer complicated the interpretation of data in that region. The measured pressure gradients $\partial p/\partial z$ (the

x (cm)	α_e°	z (cm)
3.81	0.68	3.81
4.45	1.17	3.82
5.08	1.65	3.83
5.72	2.29	3.85
6.35	2.65	3.88
6.99	3.16	3.91
7.62	3.67	3.94
8.26	4.18	3.99
8.89	4.71	4.03
9.53	5.24	4.08
10.16	5.77	4.14
10.80	6.30	4.21
11.43	—	4.28

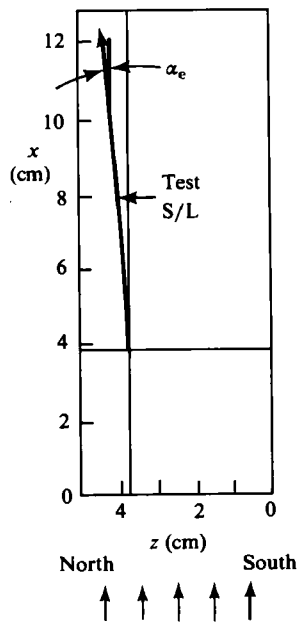

FIGURE 3. Path and coordinates of the test streamline.

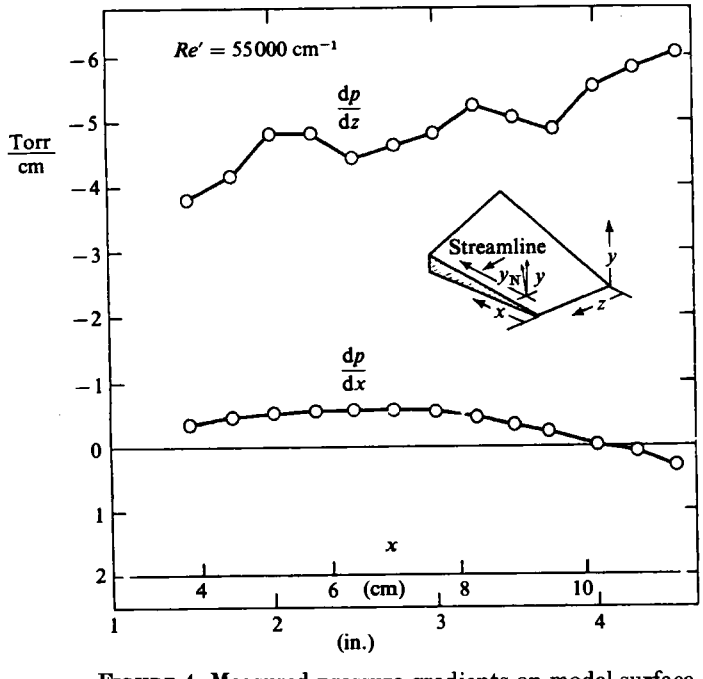

FIGURE 4. Measured pressure gradients on model surface.

TPG) and $\partial p/\partial x$ along the streamline are shown on figure 4. The desired goal of $\partial p/\partial x \ll \partial p/\partial z$ seems to have been attained. The TPG also appears to be nearly constant at 4–6 torr/cm and considerably larger than the longitudinal gradient $\partial p/\partial x$. In non-dimensional terms the averages of the gradients shown can be written as

$$|m_z| \equiv \left|\frac{\theta}{\rho_e u_e^2}\frac{\partial p}{\partial z}\right| \simeq 6\times 10^{-4}, \quad |m_x| \equiv \left|\frac{\theta}{\rho_e u_e^2}\frac{\partial p}{\partial x}\right| \simeq 6\times 10^{-5}, \tag{2}$$

or, alternatively,

$$a_z' \equiv \frac{\nu_e}{\rho_e u_\tau^3}\frac{\partial p}{\partial z} \simeq 1.5\times 10^{-3}, \tag{3}$$

where ρ, ν, u, and θ are the density, kinematic viscosity, velocity, and momentum thickness, and subscript e refers to the boundary-layer edge, and where u_τ is the friction velocity.

Since the streamline deflection, the model wedge angles and the variations of the latter were all small, considerable geometric simplifications were possible in the measurement of distances and in the data acquisition and analysis. Thus the distances x and z along and transversely across the wedge surface are approximated as parallel to their respective wind-tunnel coordinates (see figure 1), and y_N refers to the distance from the model surface along the true local vertical. The longitudinal-velocity component u and transverse component w ('crossflow') are parallel to the local surface, and respectively parallel to and perpendicular to the streamline shown on figure 3.

4. The longitudinal velocity, total temperature and shear stress

Profile measurements were made with the yawmeter and thermocouple probe at twelve positions spaced $\Delta x = 0.64$ cm apart, along the test streamline beginning at $x = 4.4$ cm. The longitudinal-velocity component and local-total-temperature data are shown on figures 5 and 6; the former is plotted in the usual $u^+(y^+)$ form of Van Driest (1955) and the latter in terms of u/u_e *vs.*

$$H \equiv \frac{T_0 - T_w}{T_{0e} - T_w}, \tag{4}$$

where T_0, T_w, and T_{0e} are the measured total, wall and stream total temperature respectively. Superposed on these figures are the 'initial' conditions in the form of profiles obtained on the tunnel floor ahead of the model.

The present initial velocity distribution obtained with the yawmeter, shown on figure 5, was found to be almost identical with that obtained earlier at the same location of this wind tunnel by Laderman (1978) using a simple pitot tube. As can be seen from figure 5, Laderman's and the present results lie very close to the 'classical' $u^+ = 5.0 + 2.43 \ln y^+$ result in the region $y^+ > 100$, but with a slightly larger intercept (6.5 *vs.* 5) and smaller slope (2 *vs.* 2.4) than the classical result. This is not a serious discrepancy, especially since the data in the 'wake' region usually make it difficult to deduce precisely the law-of-the-wall profile slope from the data. The data points shown on figure 5 belong to the three-dimensional region of the flow ($x > 4$ cm, figure 3) and here it is clear that, although the slope has not substantially changed, the profile is displaced upward and the intercept, chosen as 8.1, is visibly higher than in the two-dimensional flow ahead of the model.

On the average, the total-temperature profile in the three-dimensional region,

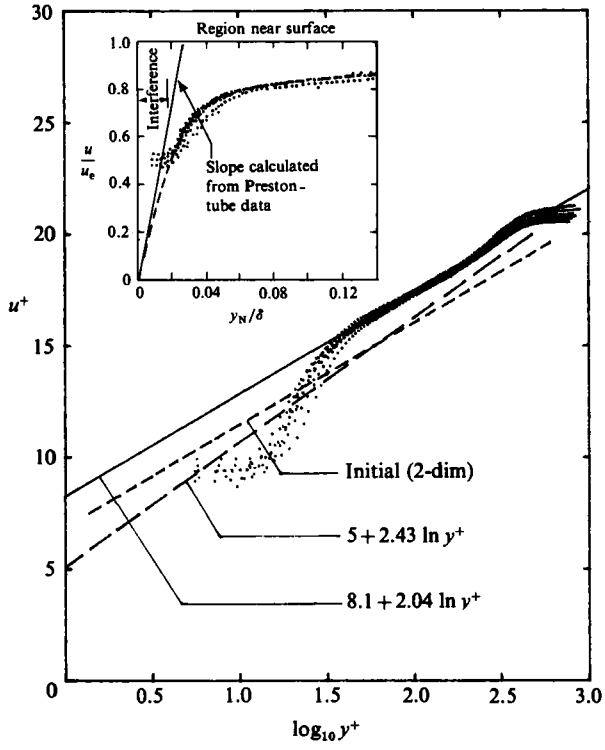

FIGURE 5. Velocity distribution in Van Driest coordinates.

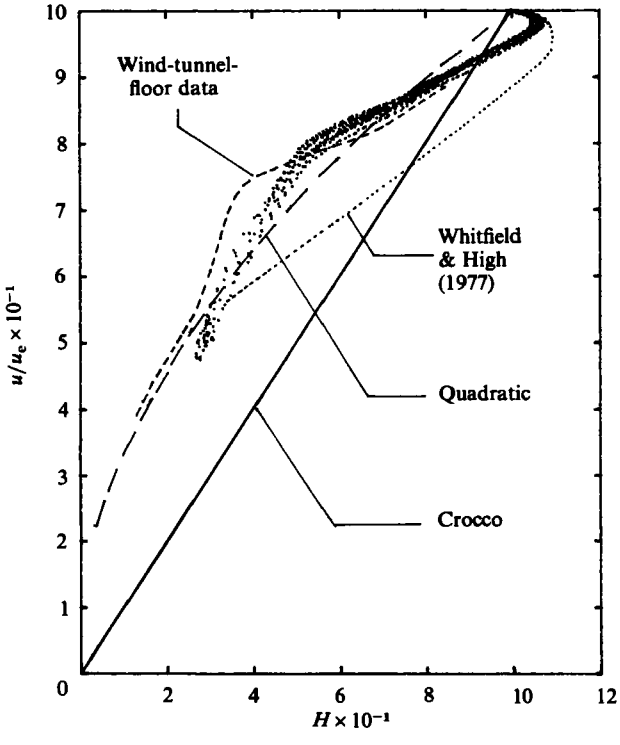

FIGURE 6. Distribution of total temperature across the boundary layer.

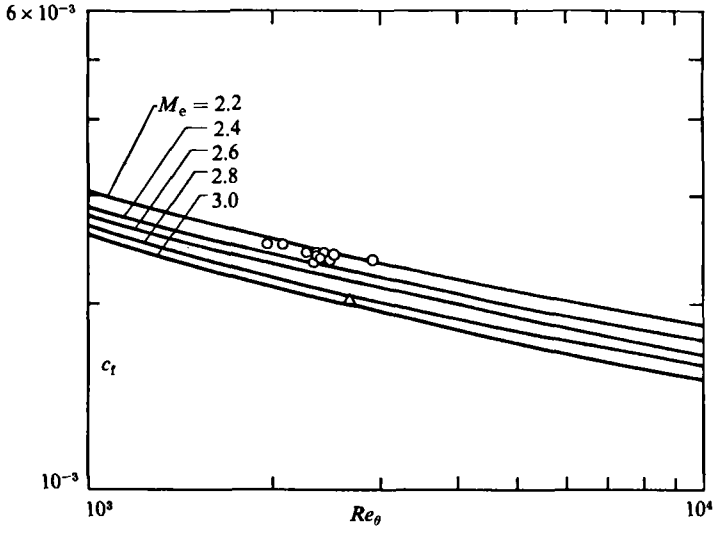

FIGURE 7. Friction coefficient results: △, Laderman (1980); solid lines, Hopkins & Inouye (1971).

Quantity	Symbol	Average	Variation
Streamwise distance	x (cm)	—	4.4–11.8
Boundary-layer thickness	δ (cm)	0.88	0.73–0.95
Momentum thickness	θ (cm)	0.033	0.029–0.035
Static pressure	p (torr)	—	25–27.2
Edge velocity	u_e (m/sec)	619	—
Mach number	M_e	2.81	2.77–2.87
Momentum Reynolds number	Re_θ	2394	—
Maximum deflection angle†‡	α_w°	4.9	4.6–5.2
Inviscid wall angle†	α_0°	1.4	0.8–1.7
True maximum deflection angle†‡	$\alpha_0 - \alpha_w^\circ$	3.5	3.2–4.1
Maximum crossflow‡	w_w/u_e	0.068	0.054–0.073
True maximum crossflow‡	w_{wT}/u_e	0.06	0.05–0.075
Friction coefficient	c_f	0.00245	—
Pressure gradient	m_z	0.000595	—
Pressure gradient	a_z'	0.00155	—

† Referred to the boundary-layer edge. ‡ At the sublayer edge.

TABLE 1. Flow properties along test streamline

represented by the points on figure 6, changes very little from the form it was found to have on the floor ahead of the model. The latter, in turn, is again very similar to the data obtained by Laderman (1978) at the same position ahead of the model. It is also evident from figure 6 that there is a considerable difference between the simple linear ('Crocco') relation and the present H–u/u_e data. This type of difference, earlier attributed to nozzle–wall non-equilibrium effects (Bertram & Neal 1965), has now been convincingly attributed by Laderman (1978) to the neglect of the viscous stresses in the Crocco model through the assumption of unity Prandtl number. Data

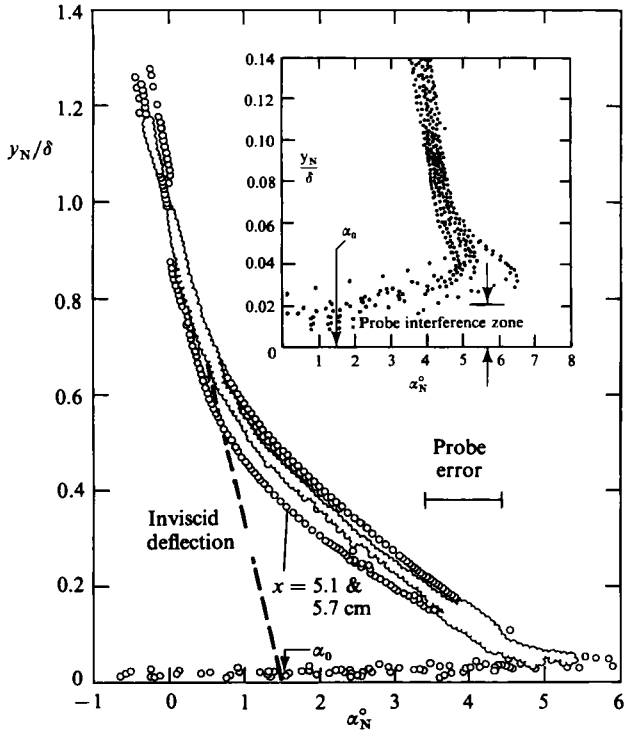

FIGURE 8. Flow deflection angle in the boundary layer.

of Laderman support the 'quadratic' $H(u/u_e)$ relation of Walz (1962) and the recent theory of Whitfield & High (1977), which includes shear-stress modelling, non-unity Prandtl number and heat transfer, and which indicates that the 'linear' Crocco relation obtains only for cooled walls.

Sufficient resolution was available in the present measurements to discern the viscous sublayer, which appears systematically in the aggregate of data shown in the insert of figure 5. Closer to the wall, a region appears where the data give a finite velocity; this region, amounting to one half the sublayer thickness, is almost equal in height to the yawmeter-probe diameter and is therefore identified with a probe–wall interference anomaly. Outside this region the velocity rate of change conforms numerically with expectations from the shear measurements illustrated on figure 7. The friction coefficients along the test streamline are about 20 % higher than found for the corresponding two-dimensional layer (Laderman 1978), but, since the Preston tube had also been aligned with the test streamline, it is safe to state that the friction component in the x-direction did not change much from that encountered in two-dimensional flows. These friction coefficients are included in table 1 which presents the average of properties measured along the streamline and their variations.

5. The crossflow component

The flow incidence angle α_N and crossflow-velocity component w are defined relative to their values at the boundary-layer edge $y_N = \delta$, so that $\alpha_N(y_N = \delta) = 0$ and $w(y_N = \delta) = 0$. This definition is essential because of the inviscid streamline deflection found between the wall leading-edge shock wave and the boundary-layer

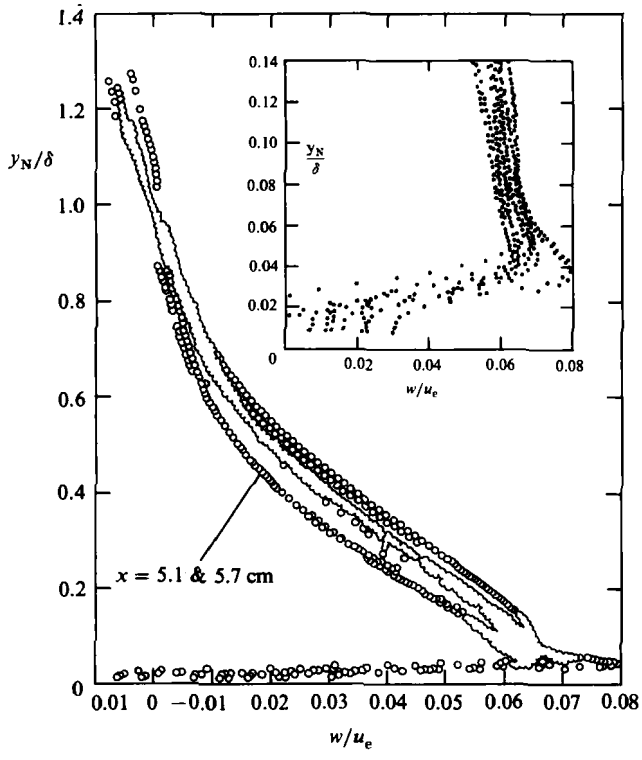

FIGURE 9. Crossflow-velocity component in the boundary layer.

edge. This deflection is caused by the wedge-model twist and is visible on figures 8 and 9, in which α_N and w/u_e are plotted *vs* the non-dimensional distance y_N/δ. The progressive increase of α_N and w toward the wall, shown in these figures, bears the expected resemblance with the supersonic-flow data of Hall & Dickens (1968) and with expectations from low-speed experiments (e.g. East 1973; Vermeulen 1971). Equally expected is the decrease of w toward zero within the sublayer, but not necessarily the similar decrease of α_N shown on figure 8, for which no adequate explanation is readily available. The maximum w and α_N values at the sublayer edge are included in table 1.

Early investigations of turbulent three-dimensional boundary layers such as done by Mager (1952), Cooke (1958), and Braun (1959) concluded that the crossflow component obeys a so-called parabolic variation of the form

$$\frac{w}{u} = \left(1 - \frac{y_N}{\delta}\right)^2 \tan \alpha_w, \tag{5}$$

where α_w is the flow deflection 'at the wall'. In their experiments at supersonic speeds, Hall & Dickens (1969) concluded that the parabolic law does not hold. Attempts to fit the present data to this law were initially impeded by the fact that the deflection angle α_N was, as previously noted, found to peak at the sublayer edge; useful results were obtained, however, when this maximum deflection angle at the sublayer edge was used in lieu of the 'wall' angle α_w, and these are shown on figure 10. The data on figure 10(*a*), which plots $w/u \tan \alpha_w$ *vs.* $(1 - y_N/\delta)^2$, should fall on a straight line joining the points (0, 0) and (1, 1) if (5) is valid. Although a semblance to a straight

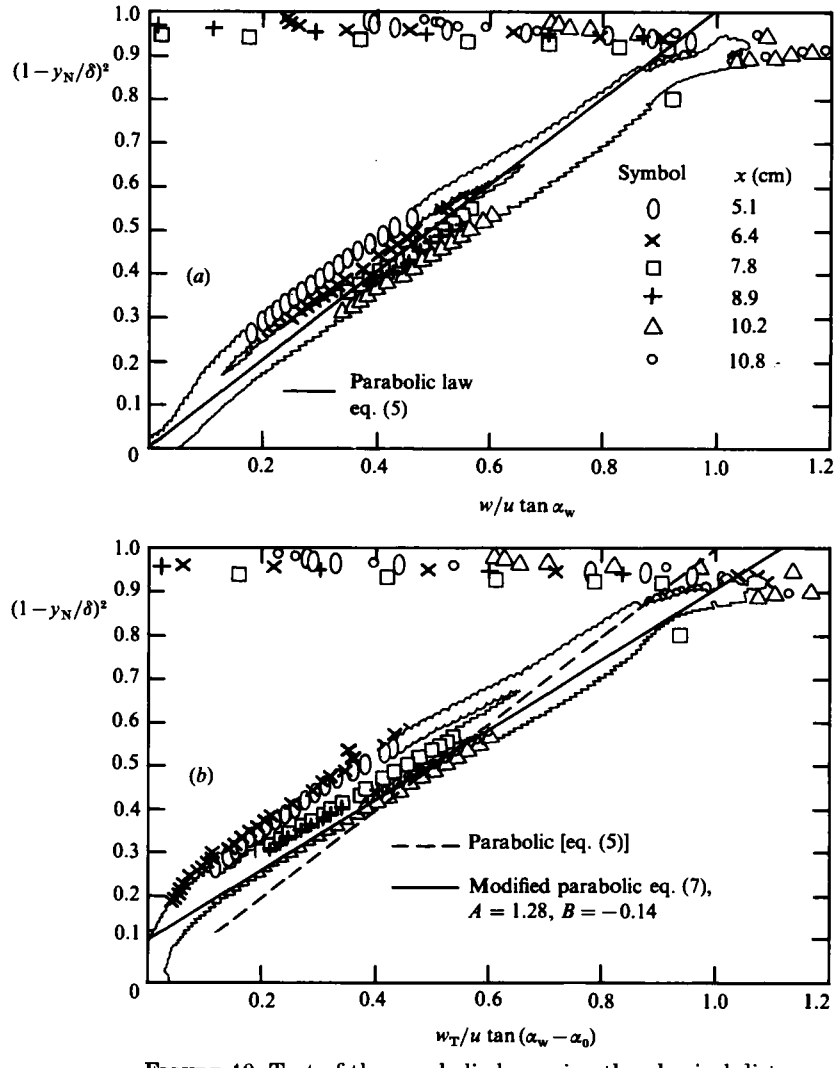

FIGURE 10. Test of the parabolic law using the physical distance: (*a*) measured crossflow; (*b*) true crossflow.

line appears toward the larger x, this line has an intercept and slope not agreeing with (5).

It is observed on figures 8 and 9 that α_N and w are finite and linearly variable outside the boundary layer, owing of course to the presence of the TPG in the inviscid flow outside the latter. One can thus hypothesize that even in the absence of the boundary layer there would be an 'inviscid' flow deflection α_i near the wall, such as shown for example by the dashed line on figure 8, which has the form

$$\alpha_i = \alpha_0\left(1-\frac{y_N}{\delta}\right), \tag{6}$$

where α_0 can be termed the 'inviscid wall angle' to signify the deflection at the wall in the absence of the boundary layer (the values of α_0 so found are given on table 1).

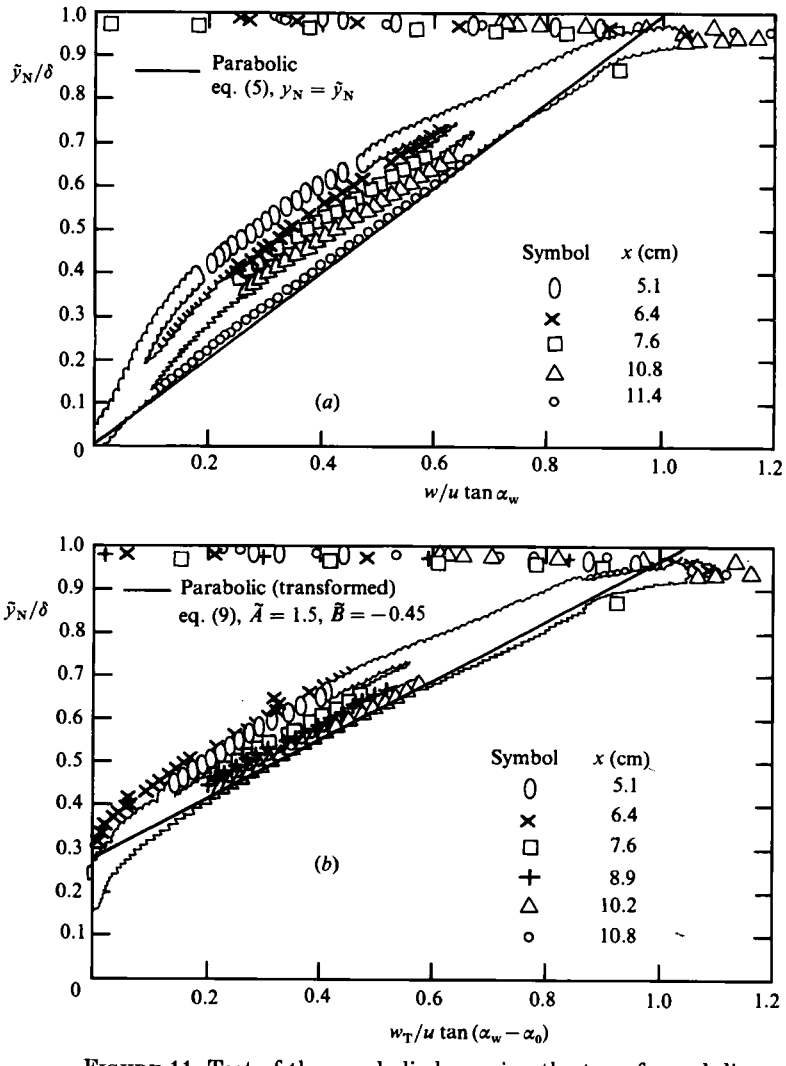

FIGURE 11. Test of the parabolic law using the transformed distance: (*a*) measured crossflow; (*b*) true crossflow.

The true deflection of the flow at the wall, including the effect of the boundary layer, therefore is $\alpha_w - \alpha_0$. The comparison discussed in the last paragraph can then be improved by computing the 'true' deflection angle $\alpha_T = \alpha_N - \alpha_i$ from the data, and the true crossflow w_T from α_T and the measured total velocity. These results can then be compared again with (5) modified to include the effect of the inviscid deflection:

$$\frac{w_T}{u \tan(\alpha_w - \alpha_0)} = A\left(1 - \frac{y_N}{\delta}\right)^2 + B. \tag{7}$$

Theoretically the quantities A and B have values 1 and 0 respectively, but the comparison with the data on figure 10(*b*) shows that $A = 1.28$ and $B = -0.14$ in $0.15 < (1 - y_N/\delta)^2 < 0.8$ (or $0.1 < y_N/\delta < 0.6$), serving to indicate that the flow deflection due to the boundary layer alone is confined below a y_N of about 0.6δ.

Since (5) was originally formulated for incompressible flows (Mager 1952) it is also appropriate to examine the compressibility effect by replacing y_N by

$$\tilde{y}_N \equiv \int_0^{y_N} \frac{\rho}{\rho_e} \, dy_N, \tag{8}$$

and comparing it with the data points transformed in the same manner. Figure 11 (*a*) shows that, toward the end of the range examined, the data are in agreement with such a 'transformed' parabolic law. One can go a step further and propose a general modification of the parabolic behaviour (5) which accounts both for the effect of the transformed coordinate y_N as above, and also for the inviscid deflection in a manner analogous to (7):

$$\frac{w_T}{u \tan(\alpha_w - \alpha_0)} = \tilde{A}\left(1 - \frac{\tilde{y}_N}{\delta}\right)^2 + \tilde{B}, \tag{9}$$

with $\tilde{A} = 1$ and $\tilde{B} = 0$. According to figure 11 (*b*), this final modification gives the best correlation of the data with the parabolic behaviour but with $\tilde{A} = 1.5$ and $\tilde{B} = 0.45$ (solid line on figure 11*b*) which again signify that the true deflection due to the boundary-layer effect is limited to $\tilde{y}_N < 0.45\delta$.

The data were also used to test the validity of the observation by Johnston (1957) that a polar plot of the crossflow *vs.* the longitudinal-velocity component yields a simple linear relationship:

$$\frac{w}{u_e} = C_1\left(1 - \frac{u}{u_e}\right), \tag{10}$$

where $C_1 = \text{const}$. The quantities w/u_e and w_T/u_e, respectively, are plotted on figures 12 (*a*) and 12 (*b*) *vs.* u/u_e. There is a semblance of straight-line behaviour of the data only near the forward portion ($x = 5.1$ cm) of the test streamline, but thereafter the points deviate from the straight line, showing that the 'Johnston triangle' cannot predict the flow behaviour for this configuration.

The present data can also be used to test the law of the wall for the crossflow proposed by Van Den Berg (1975), in which the non-dimensional TPG appears explicitly. When longitudinal-pressure gradients are absent Van Den Berg obtained a series solution for the crossflow and deflection angle of which the principal terms for small $a_z' y^+ (a_z' y^+ \ll 1)$ are

$$U_z^+ \equiv \frac{w_w - w}{u_\tau} = \frac{1}{k} a_z'(y^+ + b), \tag{11}$$

$$\phi \equiv \alpha_w - \alpha_N = \frac{a_z'(y^+ + b)}{\ln y^+ + A}, \tag{12}$$

where y^+ is the usual $y_N u_\tau / \nu_w$, b is an empirical constant to be found from the data, and where k and A are associated with the usual simple law of the wall:

$$u^+ \equiv \frac{u}{u_\tau} = \frac{1}{k}(\ln y^+ + A). \tag{13}$$

The quantities w_w and α_w signify the finite (maximum) crossflow and turning angle at the 'wall' which in this case correspond to the maximum found at the sublayer edge.

Figure 13 and 14 summarize the comparison between the present data and Van Den Berg's 'law of the wall'. To best illustrate the results, the crossflow component

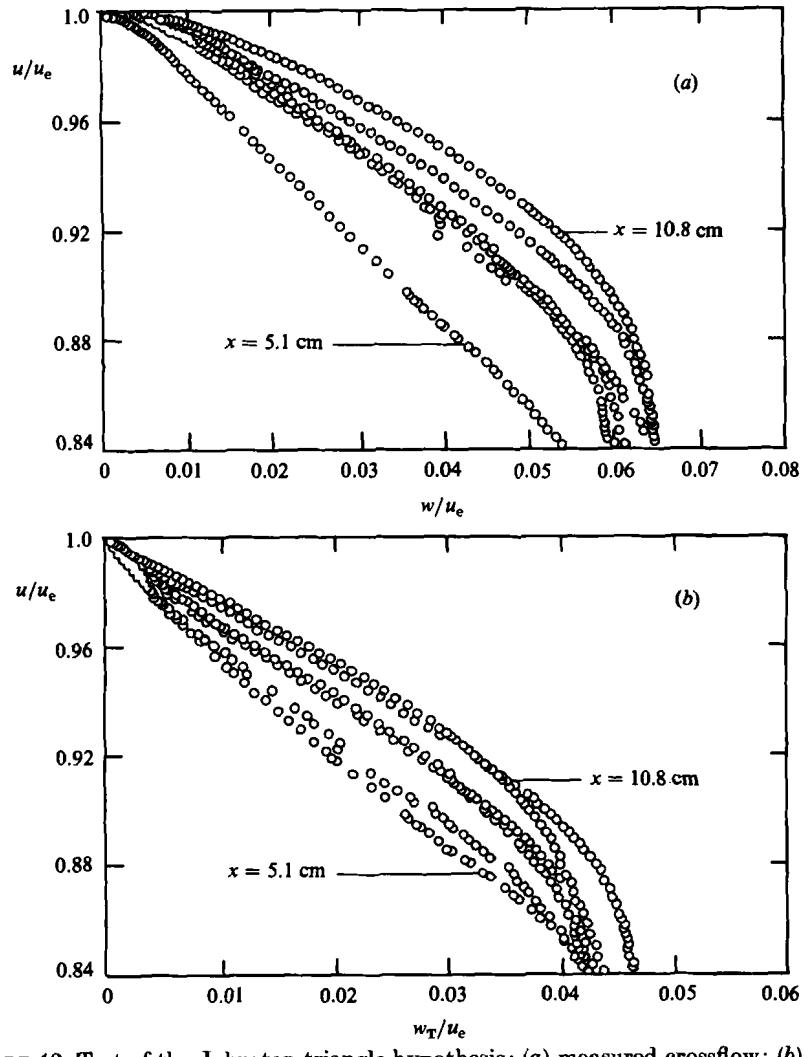

FIGURE 12. Test of the Johnston triangle hypothesis: (*a*) measured crossflow; (*b*) true crossflow.

and deflection angle have been plotted on figure 13 (using w_w and α_w as measured on the sublayer edge) as

$$\frac{w_w - w}{u_\tau a_z'} \; vs. \; y^+, \tag{14}$$

$$\frac{\alpha_w - \alpha_N}{a_z'} (\ln y^+ + A) \; vs. \; y^+, \tag{15}$$

so that if (11) is valid the former plot should have a slope of $1/k$, while the latter plot should have a slope of unity according to (12). The quantities $1/k$ and A were obtained from what appeared to be the best fit for the law-of-the-wall curve on figure 5, i.e. from $u^+ = 8.1 + 2.04 \ln y^+$, so that $1/k = 2.04$.

It is seen from figure 13 that the linearity predicted by (11) and (12) holds up to a value of y^+ of order 300, for which the 'small' parameter $a_z' y^+$ is about 0.5. On figure 13(*b*), the slope of unity predicted by (12) is attained by $x = 11.4$ cm, while in

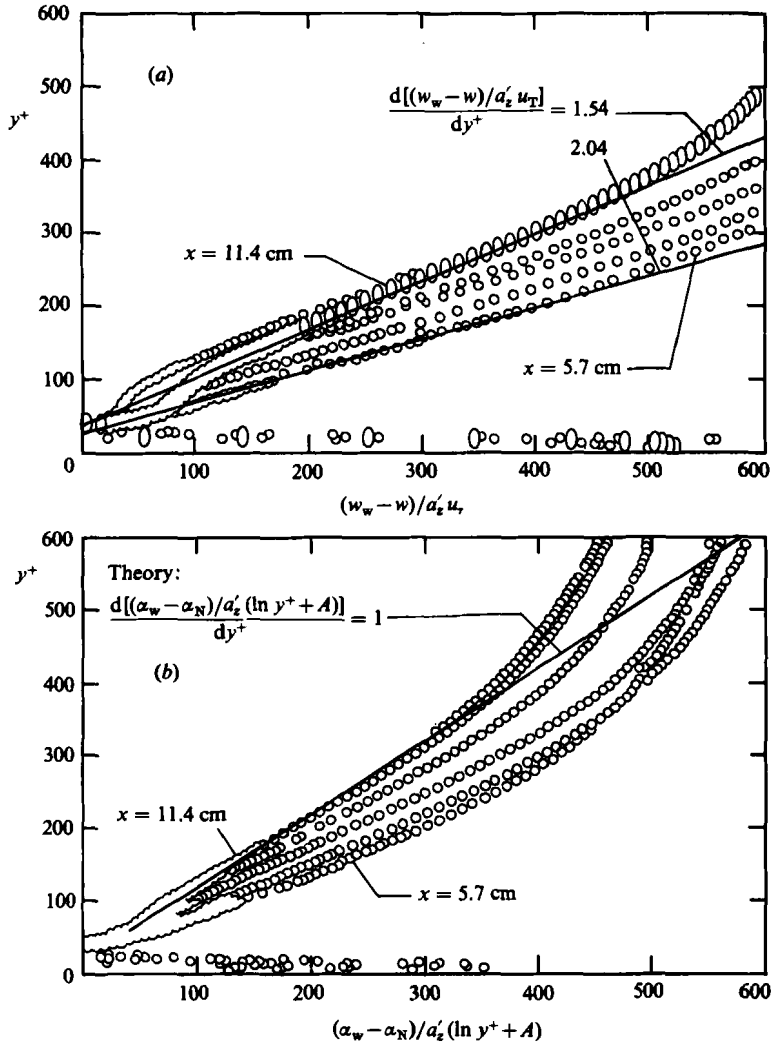

FIGURE 13. Test of the Van Den Berg predictions: (*a*) the measured crossflow, (*b*) the deflection angle.

figure 13(*a*) the data are contained within slopes ranging from the predicted 2.04, to 1.54. The constant b is found to have at most a value of -40.

To complete the description of the crossflow one must relate the key parameters appearing in the parabolic law and in Van Den Berg's formulas, with the TPG magnitude. Such an approximate empirical relation can be found, for example, by correlating small observed variations in the maximum crossflow w_w (at the sublayer edge) with similar systematic variations in m_z (see (3)):

$$\frac{w_w \rho_e u_e}{\theta}\left(\frac{\partial p}{\partial z}\right)^{-1} \simeq 114, \tag{16}$$

where θ is the local momentum thickness, and where it is assumed that $w_w(\partial p/\partial z = 0) = 0$. Alternatively, Van Den Berg observed a maximum flow deflection

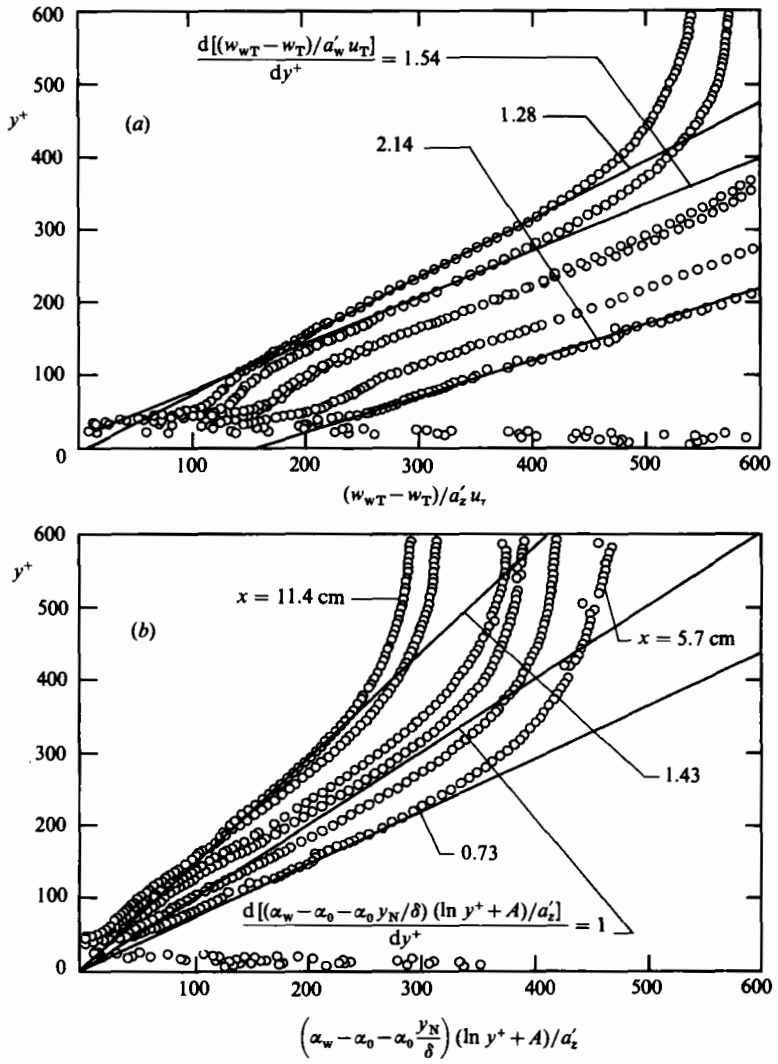

FIGURE 14. Test of the Van Den Berg predictions: (*a*) the true crossflow, (*b*) the true deflection angle.

α_w (or $\alpha_w - \alpha_0$ in the present notation) of about 10° for a TPG with a value $a'_z = 5 \times 10^{-3}$. Combining this finding with the present data and the fact that $\alpha_w(a'_z = 0) = 0$ gives

$$\alpha_w - \alpha_0 \simeq 2300 a'^{\circ}_z.$$

6. Concluding discussion

The objective of this work has been to test the early analytic approaches to the three-dimensional boundary layer, of which the parabolic variation had been a prime example. The supersonic data of Hall & Dickens (1968) showed little resemblance to such a parabolic variation, but in the present instance this variation is confirmed on figure 11(*b*) if one accounts for (*a*) the inviscid turning of the streamlines, (*b*) the compressibility transformation of the normal coordinate y^+ and (*c*) some relaxation

adjustment in the streamwise direction. A major factor for this 'reinstatement' of the parabolic profile, which could explain the difference with the Hall–Dickens data, is that in the present experiment the TPG remained nearly constant. Apparently some finite distance is required, under constant boundary conditions, for the turbulent flow to adjust to the parabolic law. However, the relaxation distance may also be characteristic of the low momentum Reynolds number (about 2500, table 1) of this experiment. This distance was of order 10δ, beginning from the leading edge of the model.

Van Den Berg's formulation gives a linear variation of the crossflow and deflection angle defined, according to (11) and (12), relative to their values on the wall. This formulation is actually a simple one, based on the inclusion of the inertial forces on the shear-stress variation, the assumption that the usual mixing-length relation holds and that the shear-stress direction coincides with the direction of deformation, and the neglect of diffusion. The results of figure 13 indicate that this approach has a certain validity, but still leaves room for relaxation effects as mentioned above.

It is difficult to rationalize, at this point, the observation that the turning angle decreases between the sublayer edge and the wall. The data shown on figures 8 and 9 make it hard to believe that this observation can be dismissed on the basis of probe–wall interference alone, and there is no sublayer data available at low speeds for comparison. If true, this phenomenon would imply that the streamline direction on the wall is close to the streamline direction at the boundary-layer edge, and would complicate profoundly the shear-stress distribution in the sublayer.

In summary, the results of these measurements indicate that:

(1) A constant transverse pressure gradient with non-dimensional magnitude of about 1.5×10^{-3} was found to increase the intercept and to decrease the slope of the 'law of the wall' in a turbulent supersonic boundary layer. The same gradient also increased the friction coefficient by about 20% over the corresponding value for a two-dimensional boundary layer.

(2) The crossflow component and flow-deflection angle attained a self-similar form over a streamline length of about 10 layer thicknesses, and both increased toward the surface as observed during earlier experiments. The deflection angle, however, was observed to decrease again in the viscous sublayer. The maximum crossflow and deflection angle in the layer were empirically connected to the transverse-pressure-gradient magnitude.

(3) Comparison between the data and the so-called parabolic law for the crossflow component showed that agreement between the two exists past a streamwise relaxation distance, provided that one accounts for the inviscid flow deflection and that the distance from the wall is contracted by the compressibility transformation. Accounting for the inviscid flow deflection reveals that the turning of the flow due to the boundary layer alone, is again limited to the bottom half of the layer as at low speeds.

(4) The data also compare well with Van Den Berg's extended 'law of the wall', which is typical of analytic approximations of incompressible three-dimensional boundary-layer behaviour. This comparison is favourable for values of the y^+ coordinate up to 300.

This research was supported by the National Aeronautics and Space Administration, Ames Research Center, under NASA Grant NAG 2-37.

REFERENCES

Bradshaw, P. & Unsworth, K. 1974 *AIAA J.* **12**, 1293.

Braun, W. H. 1959 *NACA TN* 4208.

Cooke, J. C. 1958 *Aero Res. Counc. RM* 3199.

Demetriades, A. & McCullough, G. H. 1982 *Montana State Univ. Rep. SWT TR* 82–04.

East, L. F. 1973 *Aero Res. Counc. RM* 3768.

Fanneløp, T. K. & Krogstad, P. A. 1975 *J. Fluid Mech.* **71**, 815.

Hall, M. G. & Dickens, H. B. 1968 *Aero Res. Counc. RM* 3537.

Hopkins, E. J. & Inouye, M. 1971 *AIAA J.* **9**, 993.

Johnston, J. P. 1957 *MIT Gas Turbine Lab Rep. No.* 39.

Laderman, A. J. 1978 *AIAA J.* **16**, 723.

Laderman, A. J. 1980 *AIAA J.* **18**, 1186.

Mager, A. 1952 *NACA TN* 1067.

Rastogi, A. K. & Rodi, W. 1978 *AIAA J.* **16**, 151.

Spaid, F. W., Hurley, F. W. & Helman, T. H. 1975 *AIAA J.* **13**, 253.

Van Den Berg, B. 1975 *J. Fluid Mech.* **70**, 149.

Van Driest, E. R. 1955 *50 Years Boundary Layer Research*, p. 257. Vieweg.

Vermeulen, A. J. 1971 Measurements of three-dimensional turbulent boundary layers. Ph.D. Thesis, Cambridge.

Walz, A. 1962 *Mécanique de la Turb.*, p. 300. CNRS Paris.

Whitfield, D. L. & High, M. D. 1977 *AIAA J.* **15**, 431.

Yanta, W. J., Ausherman, D. W. & Hedlund, E. 1982 *AIAA Paper No.* 82–0289.